Editors' Suggestion

Observation of broken inversion and chiral symmetries in the pseudogap phase in single- and double-layer bismuth-based cuprates

Sejoon Lim,[1,2,*] Chandra M. Varma,[3,†] Hiroshi Eisaki,[4] and Aharon Kapitulnik[1,2,5]
[1]*Department of Applied Physics, Stanford University, Stanford, California 94305, USA*
[2]*Stanford Institute for Materials and Energy Sciences, SLAC National Accelerator Laboratory, 2575 Sand Hill Road, Menlo Park, California 94025, USA*
[3]*Physics Department, University of California, Berkeley, California 94704, USA*
[4]*National Institute of Advanced Industrial Science and Technology, Tsukuba, Ibaraki 305-8568, Japan*
[5]*Department of Physics, Stanford University, Stanford, California 94305, USA*

(Received 5 December 2021; revised 6 February 2022; accepted 7 March 2022; published 4 April 2022)

We deduce the symmetry of the pseudogap phase in the single- and double-layer bismuth-based cuprate superconductors, where charge and pseudogap order onset concurrently, by measuring and analyzing their circular and linear photogalvanic responses, which are related *linearly* to the chirality and inversion breaking, respectively, of the order parameter. After separating out the trivial contribution arising from the surface where inversion symmetry is already broken, we show that both responses start below the pseudogap temperature T^* and grow below it to a sizable magnitude, revealing the broken symmetries in the bulk of the crystal. Through a detailed analysis of the dependence of the signals on the angle of incidence, the polarization of the light, and the orientation of the crystal, we are able to discover that the point group symmetry below T^* is limited to $mm2$ or $mm2\underline{1}$ groups. Taking into account formation of domains and previous measurements, our results narrow down the possible symmetries of the microscopic origin of the phase transition(s) at T^*, which leads to the conclusion that while charge order may affect the observed symmetry it is not the main cause of the pseudogap order parameter.

DOI: 10.1103/PhysRevB.105.155103

I. INTRODUCTION

One of the long-standing questions in the study of the high-T_c cuprate superconductors is the understanding of the nature of the boundary between the strange metal phase and the pseudogap phase [1]. Over the years, it has become increasingly evident through experimental findings that this boundary marks a true phase transition, initially suggested in [2] proposing the so-called loop-order model, with the subsequent range of models exhibiting magnetic (e.g., [3]) or charge order (for a review see, e.g., [4]). Some of the observed broken symmetries in the canonical yttrium- and bismuth-based cuprates, for example, include time reversal [5–12], fourfold rotation [13–23], translation [14,16–18,20–22,24], inversion [12], or a combination of these [5,7–12]. However, while all those experiments contribute to constraining the symmetry of the pseudogap phase in these compounds, it is not yet considered fully understood. In particular, the question of interplay between structural and electronic effects in BSCCO where charge and pseudogap order onset concurrently (e.g., [9,21,22]) needs to be sharpened up.

In this paper, we report circular (CPGE) and linear (LPGE) photogalvanic effects (PGE) [25–27] in single crystals of near optimally doped single- and double-layer bismuth-based cuprate superconductors (BSCCO): $Pb_{0.55}Bi_{1.5}Sr_{1.6}La_{0.4}CuO_{6+\delta}$ (Pb-Bi2201) with $T_c \approx 38$ K and $Bi_{2.1}Sr_{1.9}CaCu_2O_{8+\delta}$ (Bi2212) with $T_c \approx 86$ K, previously used in studies in our group, where the location of the pseudogap was clearly identified [9,28]. While the PGE originating from the "trivial" inversion-symmetry breaking of the probed surface is present already at temperatures above T^*, an additional signal with onset near the pseudogap temperature T^* and growing with decreasing temperature is clearly discerned. Here we present evidence that the appearance of this "nontrivial" PGE across T^* points to inversion-symmetry breaking and chirality in the pseudogap phase of BSCCO, which is robust to spatial averaging of structural domains. The CPGE and LPGE observed are linear in the photon intensity and therefore linear in the order parameter characterizing the broken symmetry of the pseudogap phase, unlike almost all the scattering experiments mentioned above. This allows us through a comprehensive symmetry analysis of the experiments to deduce more details of the symmetry than other techniques which have been used to date.

The PGE is the dc current measured in response to photon intensity with specified polarization and angle of incidence:

$$j_i = \chi_{ijk}(E_j E_k^* + E_j^* E_k)/2 + i\gamma_{il}(\vec{E} \times \vec{E}^*)_l, \qquad (1)$$

where $\vec{E}$ is the complex amplitude of the electric field with components $\{E_i\}$ and intensity $I = |\vec{E}|^2$. The CPGE is characterized by the second-rank axial tensor γ_{il}, and the LPGE by the third-rank polar tensor χ_{ijk} [29]. Both effects are absent in centrosymmetric media. In Eq. (1), effects due to photon drag and sample heating are not included.

*lims@stanford.edu
†Recalled professor.

The summary of our observations of the nontrivial PGE is as follows: (i) We observe chirality in both the CPGE and LPGE; i.e., the direction of current in the plane is rotated with respect to the plane of incidence and its sign is invariant to the in-plane rotation of the crystal. (ii) Both the in-plane CPGE and LPGE are observed only at oblique incidence of radiation. (iii) At normal incidence, only the c-axis LPGE is observed. (iv) The magnitude of the PGE is of the order of the surface-induced PGE for Bi2212 and several times larger for Pb-Bi2201. In addition we show that (v) the CPGE and LPGE in the overdoped regime follow similar behavior; (vi) measurements on Bi2212 at much higher photon energy, where neither intraband nor interband effects are pronounced [30–32], show very weak (if any) PGE signal.

These observations and the detailed dependence of j_i on the angle of the plane of incidence of the photons and their polarization provide 11 different criteria which are used to discern background effects and thus discover the point group symmetry of the pseudogap phase after an examination of the predictions for all the relevant 34 groups. These groups and their consistency with each of the 11 properties or otherwise are listed in Table S1 in the Supplemental Material (SM) [33].

II. EXPERIMENT

Two-terminal BSCCO devices were fabricated as described in the SM [33], and mounted on the PGE apparatus as illustrated in Fig. 1(a), which also depicts the convention we use for the crystallographic axes. Electrical resistance as a function of temperature was first measured to characterize the samples and obtain an estimate of T^* by locating the point of deviation from linear resistivity (see, e.g., [34]). Typical resistance curves for Pb-Bi2201 with $T_c \approx 35$ K and $T^* \approx 130$ K and Bi2212 with $T_c \approx 87$ K and $T^* \approx 200$ K are shown in Figs. 1(b) and 1(c), respectively. For Pb-Bi2201, our derivation of $T^* \approx 130$ K agrees with the measurements by angle-resolved photoemission spectroscopy, the polar Kerr effect, and time-resolved reflectivity [9], which were carried out on the same batch of crystals used in this study. Bi2212 crystals similar to ours were recently studied in [35], where $T^* \approx 200$ K was determined for near optimally doped and $T^* \approx 150$ K was reported for overdoped samples with $T_c \approx 77$ K, which we report in the SM [33].

PGE measurements were carried out for a fixed angle θ at either normal ($\theta = 0°$) or oblique ($\theta = 40°$) incidence of radiation at 1550 nm, which lies within the intraband transport regime for both BSCCO phases [30–32]. The photoinduced dc electric currents were measured using a lock-in technique by chopping the excitation light at a frequency of 737 Hz. The plane of incidence is oriented perpendicular to the pair of electrical contacts as illustrated in Fig. 1(a). Its orientation relative to the crystallographic axes, represented by the azimuthal angle ϕ, is therefore determined by the current direction. For example, $\phi = 0$, $\pi/4$, and $\pi/2$ correspond to the configurations where the currents are measured along the y axis in the direction of the superstructural modulation [36], Cu-O bond direction, and x axis, respectively. For each fixed θ and ϕ, the currents were measured as a function of the phase angle φ, which is the rotation angle between the plane of the initial p polarization and the optical axis of a quarter-wave plate. Emphasizing the CPGE, we use a quarter-wave plate, rotating it continuously to scan between right and left circular polarizations. Thus, in our experiment information about the LPGE is extracted from the intermediate polarizations that vary between purely linear in the incidence plane to elliptical at an arbitrary angle.

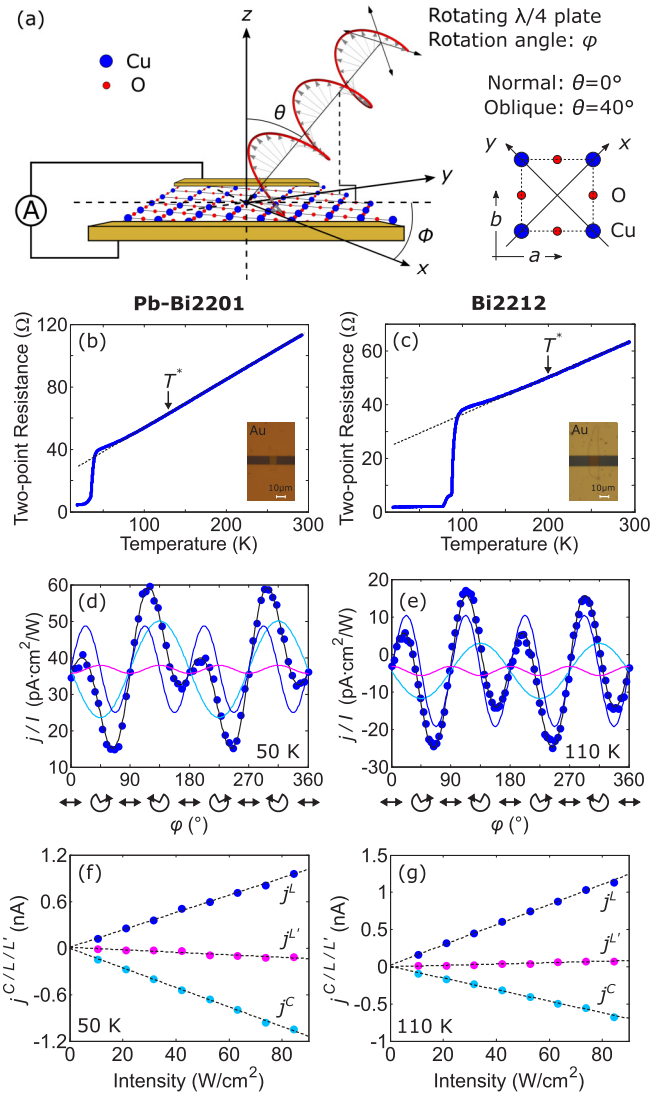

FIG. 1. Measurements of the in-plane electrical resistance and photoinduced electric current on a 70 nm thick Pb-Bi2201 device and a 100 nm thick Bi2212 device. (a) Schematic of the experimental geometry. (b), (c) Two-point electrical resistance of (b) Pb-Bi2201 and (c) Bi2212 as a function of temperature. The insets show optical images of the measured devices. (d), (e) Photoinduced electric current measured at (d) 50 K in Pb-Bi2201 and at (e) 110 K in Bi2212 as a function of the phase angle φ. The measurements were carried out under oblique incidence of radiation. In each plot, the black line shows a fit to the phenomenological equation, while the light blue, blue, and magenta lines show the components proportional to $\sin 2\varphi$, $\sin 4\varphi$, and $\cos 4\varphi$, respectively. (f), (g) Intensity dependence of j^C, j^L, and $j^{L'}$ in (f) Pb-Bi2201 and (g) Bi2212.

Figures 1(d) and 1(e) show typical measurements carried out under oblique incidence at temperatures near but above T_c. Overall, these currents share a fairly similar dependence

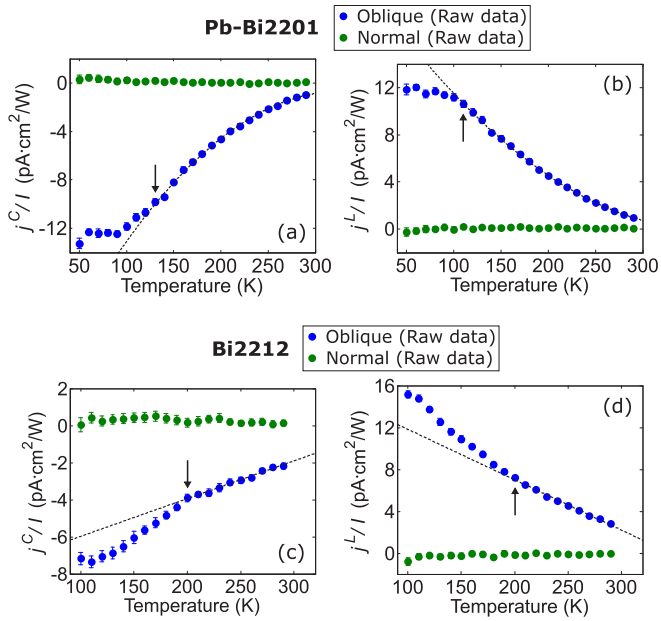

FIG. 2. Temperature dependence of j^C and j^L, normalized by the light intensity I, in the Pb-Bi2201 and Bi2212 samples characterized in Fig. 1. The error bars represent 95% confidence intervals. The dashed black lines are guides to the eye, and the arrows mark the approximate onset of deviation from the high-temperature trend.

on the polarization of the excitation light, and are well fitted to the phenomenological equation [37]

$$j = j^C \sin 2\varphi + j^L \sin 4\varphi + j^{L'} \cos 4\varphi + d. \qquad (2)$$

Here j^C is the CPGE coefficient, while both j^L and $j^{L'}$ contain information about the LPGE. The fits of the data to the above equation exhibit the following common features: (i) j^C, j^L, and $j^{L'}$ are proportional to the light intensity as shown in Fig. 1(f) for Pb-Bi2201 and Fig. 1(g) for Bi2212. (ii) Where observed at oblique incidence, $j^C/j^L \sim O(1)$ and they follow the same temperature dependence but with opposite sign. (iii) For y-z or x-z incident planes (i.e., current measured along x or y, respectively), $j^{L'}$ is typically small, on the order of $\sim 0.1\, j^L$. (iv) Uniquely below T^*, for an incident plane rotated away from the principal axes (x or y), $j^{L'}$ becomes finite beyond its typical residuals, and may increase in magnitude to be a large fraction of j^L. We will use this information to determine that true inversion-symmetry breaking in the material is manifested by the CPGE term j^C, and by the LPGE terms j^L and $j^{L'}$ (when the two terms are of same order). The constant term d and the residuals of $j^{L'}$ are associated with the photon drag and thermal effects (see, e.g., [26] and further discussion in the SM [33]).

III. RESULTS

Figure 2 shows the temperature dependence of j^C and j^L, normalized by the light intensity I, in the Pb-Bi2201 and Bi2212 samples characterized in Fig. 1. In Pb-Bi2201, where Pb doping suppresses the superstructure in the BiO plane [9], the current direction is estimated to be along one of the principal axes, x or y. The current direction in Bi2212 is carefully aligned close to the y axis in the direction of the superstructural modulation [36] (see SM [33]). While the present paper focuses on the behavior near and below T^*, we note that close to T_c, superconducting fluctuations are noticeable, typically causing strong deviations of the PGE currents (see SM [33]).

A feature that complicates the analysis of the oblique incidence data is the occurrence of finite j^C and j^L already at room temperature, much above T^*. This may be expected due to inversion-symmetry breaking at the surface, or as a bulk effect if inversion symmetry is already broken. However, the crystal structure of Bi2212 belongs to the orthorhombic space group *Bbmb* [38–40], which has the point group symmetry *mmm* (D_{2h}) in the bulk and *mm*2 (C_{2v}) at the surface. Since *mmm* is centrosymmetric, the bulk cannot produce PGE. We therefore expect PGE only from the surface with possible contributions from intraband and interband excitations. At the same time, previous studies on the BSCCO family of cuprates suggest that free carriers dominate the optical properties at the wavelength of the light used [30,31], exhibiting nearly isotropic in-plane scattering rate. These in turn will contribute a more tetragonal-like PGE response associated with the normal to the surface vector. Such an isotropic response is indeed evident in the high-temperature part of the LPGE, where above a constant value similar to that of j^L (see below), $j^{L'}$ response along the x or y directions increases with decreasing temperature, while along the Cu-O bond direction it is temperature independent (see SM [33]). The observed monotonic and featureless variation of the surface PGE with decreasing temperature is further in agreement with the kinetic approach, where the increasing mean-free path results in the increasing PGE currents [41,42]. While the kinetic part is expected to exhibit temperature dependence, the noncentrosymmetric nature of the surface accounts for the constant offset to the observed high-temperature signal of the surface, probably through interband transitions. We thus treat the surface PGE as a baseline, above which nontrivial contributions that appear below T^* are analyzed. This approach is further justified by the self-consistent analysis, particularly that off the LPGE signal along the Cu-O direction below T^*.

Indeed, with decreasing temperature, j^C and j^L start to deviate from their high-temperature trend near T^*, indicating the appearance of nontrivial PGE currents. These relative deviations are much larger than the subtle deviations of resistivity through T^* and cannot be explained by the kinetic approach [41,42]. In addition, as our symmetry analysis will show, the experimentally determined symmetry below T^* is *mm*2 (or *mm*2$\underline{1}$), which implies that the surface symmetry does not change. Thus, both observations suggest that the additional PGE below T^* is a bulk effect. This behavior is more pronounced in Pb-Bi2201, where the rate at which j^C and j^L increase with decreasing temperature slows down below $T^* \approx 130$ K. In near optimally doped Bi2212, a similar deviation, but with opposite polarity, is observed roughly near $T^* \approx 200$ K, which is somewhat weaker in magnitude and sets in gradually over a broader temperature range. Measurements on overdoped Bi2212 with $T_c \approx 77$ K show similar deviations appearing at the respective lower $T^* \approx 150$ K (see SM [33]).

Fitting the high-temperature oblique incidence PGE data to a smooth curve, we extract the low-temperature evolution of the nontrivial component by subtracting this trivial

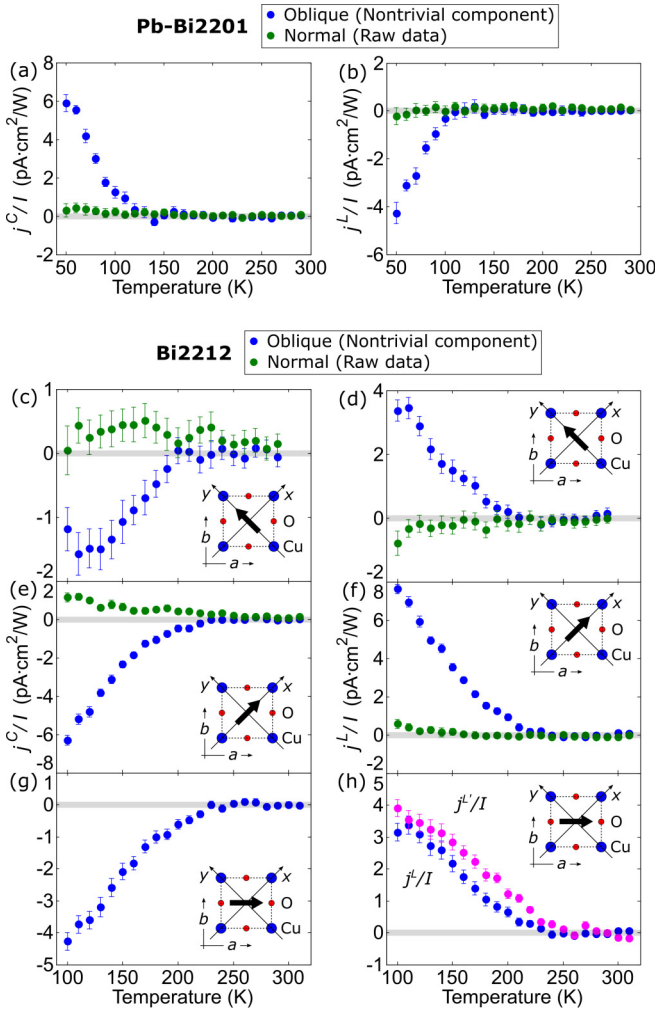

FIG. 3. Temperature dependence of j^C/I and j^L/I, where the oblique incidence data have been subtracted to show the nontrivial component of the overall current. (a), (b) Data for Pb-Bi2201 with current direction estimated along x or y. (c)–(h) Data for Bi2212 in three different configurations. Current direction aligns close to either the (c), (d) y-axis, (e), (f) x-axis, or (g), (h) Cu-O bond direction. The magenta data points in (h) represent $j^{L'}/I$ in this configuration. This LPGE term is small (hence, not displayed) in the other two configurations shown in (d) and (f) (see SM [33]). The error bars represent 95% confidence intervals.

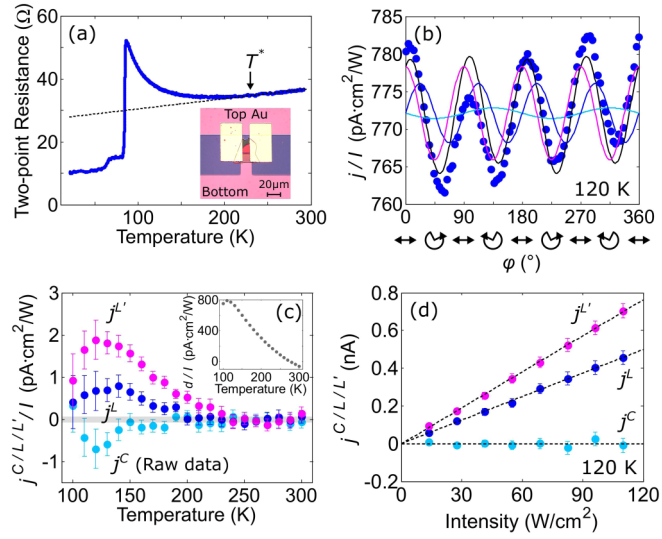

FIG. 4. Measurements of the c-axis electrical resistance and photoinduced electric current on a 90 nm thick Bi2212 device. (a) Two-point electrical resistance as a function of temperature. The inset shows an optical image of the measured device. (b) Photoinduced electric current measured at 120 K as a function of the phase angle φ. The measurement was carried out under normal incidence of radiation. The black line shows a fit to the phenomenological equation, while the light blue, blue, and magenta lines show the components proportional to $\sin 2\varphi$, $\sin 4\varphi$, and $\cos 4\varphi$, respectively. (c) Temperature dependence of j^C, j^L, and $j^{L'}$, normalized by the light intensity I. j^L and $j^{L'}$ have been subtracted to show the nontrivial component. The error bars represent 95% confidence intervals. The inset shows the temperature dependence of d/I. (d) Intensity dependence of j^C, j^L, and $j^{L'}$.

background from the overall current. Figures 3(a) and 3(b) show the nontrivial CPGE and LPGE versus temperature for Pb-Bi2201, suggesting a behavior consistent with an increasing order parameter below T^*. Figures 3(c) through 3(h) summarize the more comprehensive study carried out on Bi2212, where three different samples from the same batch are carefully aligned with current directions close to either the y-axis [(c), (d)], x-axis [(e), (f)], or Cu-O bond direction [(g), (h)] (see SM [33]). Note that normal incidence data in Fig. 3 are (unsubtracted) raw data, which seem to agree with no PGE in that configuration for either material.

Focusing on Bi2212, a key feature of all these measurements is that the nontrivial PGE currents show similar size and trend irrespective of the crystal orientation, which suggests a chiral behavior. However, cooling the sample in the presence of intense light with either right or left circular polarization prior to the PGE measurements did not yield different results, thus suggesting that no simple trainable gyrotropic effect is present (see, e.g., [43]). We are therefore led to include magnetic symmetry groups in analyzing the CPGE.

To complement the a-b plane current measurements, we also searched for PGE along the c axis in Bi2212. Figure 4 is an example of such a measurement, where Fig. 4(a) shows a typical c-axis resistance curve with $T^* \approx 230$ K marked as the point of deviation from high-temperature linear resistivity. The c-axis photocurrent measured under normal incidence of radiation at 120 K is shown in Fig. 4(b). Although there is a significant offset component arising from the photon drag and thermal effects, as well as an accompanying slight distortion in the overall wave form due to alignment imperfections, we can extract j^C, j^L, and $j^{L'}$ by following the fitting procedure of Eq. (2). Figures 4(c) and 4(d) depict the temperature and light intensity dependence of these fitting coefficients, indicating that, while small, only the LPGE occurs in this measurement geometry. The LPGE surface term above T^* is of the same order of magnitude and similar in trend to the a-b plane LPGE [33], reflecting the similar decrease in sample c-axis resistance in that regime. Thus, the sharp increase in c-axis resistance below T^* would yield a large decrease in surface LPGE in that direction, while we observe the opposite trend, confirming a nontrivial c-axis LPGE below T^*.

IV. ANALYSIS AND DISCUSSION

A. Symmetry analysis

As argued above and in the SM [33], surface effects present at room temperature cannot explain the emergence of an additional PGE below T^*, and thus we turn to the analysis of possible broken symmetries in the bulk. While the LPGE calls only for broken inversion symmetry, the observation of chirality in both the LPGE and CPGE, and the fact that time-reversal symmetry breaking has been reported for both Pb-Bi2201 [9] and Bi2212 [8,10,11], suggests that we search among the magnetic point groups including the allowed classical subgroups [44]. In carrying out symmetry analysis, we start with the general requirements for γ_{il} [41,42] and identify the possible magnetic point groups consistent with the CPGE data. Including "gray groups" (see below), this procedure yields 34 point groups in the triclinic, monoclinic, orthorhombic, and tetragonal groups, which we need to test in accord with the observations (i), (ii), and (iii) which extend to 11 properties when we take into account the angular and polarization dependencies described above. All 34 point groups are listed in Table S1 [33], together with the 11 properties and marked with the consistency or inconsistency in each group for each of the properties. In what follows we use the notations where $\underline{o}$ denotes a regular operator o combined with time reversal symmetry operator, while $\bar{n}$ denotes a n-fold rotation-inversion operator.

We first examine point groups allowed by the CPGE where the principal axis lies along the c axis (i.e., z axis). It is common to approximate the crystal structure of BSCCO as tetragonal (since orthorhombic distortions mostly affect the BiO planes with almost no effect on the CuO_2 planes [38,45]), for which the fourfold symmetry groups allowed are $\underline{4}\underline{m}\underline{m}$ and $\underline{4}$. However, the true bulk crystal of both Bi2201 or Bi2212 is orthorhombic above T^* [38–40], with a slight distortion that reduces the symmetry around the y axis, but still remain orthorhombic [46]. Thus, if we take into account this orthorhombic distortion, then $mm2\underline{1}$ and any of its subgroups ($mm2$, $\underline{m}\underline{m}2$, $\underline{m}\underline{m}\underline{2}$, $\mathrm{m}\underline{1}$, $\underline{\mathrm{m}}$, m, $2\underline{1}$, $\underline{2}$, 2, $1\underline{1}$ and 1), are also allowed, where the monoclinic subgroups may require a different principal axis (see Table S1 in SM [33]).

We next use the LPGE data to narrow down the list of groups by searching for χ_{ijk} tensors that match each of the properties of the LPGE data. Here, in addition to the requirement of chirality, a key feature in the LPGE Bi2212 data is that the coefficient $j^{L'}$ is vanishingly small along x or y (see SM [33]), but along the Cu-O direction $j^{L'} \approx j^{L}$ below T^* [see Fig. 3(h)].

Implementing these two effects, and noting that the in-plane symmetry is nearly fourfold, which suggests similar magnitude to similar tensor components, both of which are discussed at length in the SM [33], we find that only the subgroups $mm2\underline{1}$ and $mm2$ are fully consistent with both our CPGE and LPGE data.

However, we note that the PGE is proportional to the order parameter, and thus the PGE current that appears upon uniform illumination of the sample is very sensitive to mesoscopic domains which, if random, would average the PGE current to $O((d/L)^2)$, where d is the typical size of the domains and $L \sim 10\ \mu$m is the size of the illuminated sample. This issue is further discussed next.

B. The results in a broader context

Focusing on the above result, $mm2$ (C_{2v}) has the following symmetries, $1, \overline{2}_x, \overline{2}_y, 2_z$, respectively, identity, twofold improper rotation about the x and y axes, and twofold proper rotation about the z axis. $mm2\underline{1}$ is the equivalent "gray group" (see, e.g., [47]), where $\underline{1}$ represents the addition of the time-reversal operator to the group, which effectively implies that for each moment in the unit cell there is the opposite moment at the same position. Thus, a "gray group" is often used to describe an equivalent paramagnetic state within the same crystallographic group, which is invariant under time reversal. A cartoon for the smallest orthorhombic unit cell exhibiting the symmetries $mm2$ and $mm2\underline{1}$ is shown in the SM [33].

On the face of it, our analysis yields an orthorhombic symmetry for the pseudogap state, which can also be taken as nonmagnetic in origin. For example, since BSCCO above T^* is orthorhombic with the *Bbmb* space group due to a slight distortion around the y axis [48] (thus, equivalent to $mm2$ with rotation around y [40]), an electronic driven structural effect that sets in at T^*, such as a charge order or nematic transition [19,49–52], would reduce the initial orthorhombic symmetry to monoclinic (note that charge order in BSCCO appears along the Cu-O bonds, thus at 45° to the principal axes). Small enough monoclinic domains can then assemble to yield an effective $mm2$ symmetry with twofold rotation along the c axis. However, the PGE is proportional to the order parameter, and thus the PGE current that appears upon uniform illumination of the sample is very sensitive to averaging of mesoscopic domains. For random domains that carry opposite sign of the order parameter, the PGE current will be reduced by a factor of $O((d/L)^2)$, with a standard deviation $O(d/L)$, where d is the typical size of the domains and $L \sim 10\ \mu$m is the size of the illuminated sample. For the BSCCO system, a one-dimensional charge density wave with typical domain size of ∼30–100 Å has been consistently observed in both Pb-Bi2201 [9,18] and Bi2212 [16,17,20–22] below the pseudogap state. Such small domains would predict a $\sim 10^{-4}$ to 10^{-3} and often much larger reduction of the single domain signal, which would make the PGE signal impossible to observe. We note that compared to "standard" materials, the typical free carrier CPGE in tellurium [53,54] or LPGE in heavily doped GaAs [55] is at most a factor of 10 larger than our nontrivial PGE values.

Thus, any smaller, monoclinic domains that assemble to exhibit $mm2$ at the mesoscopic scale must be of a certain type as to avoid a reduction of PGE currents inside a domain. In our system the key issue will be to maintain the intrinsic chirality of the domains at the sample scale. Solving this issue will also help to understand previous observation of x-ray natural circular dichroism (XNCD) that appears below T^* [56], and was argued to demonstrate that time-reversal symmetry is preserved in the pseudogap phase of underdoped Bi2212. These results were initially demonstrated to be inconsistent with only a crystal structure effect, without time-reversal symmetry breaking (TRSB) [40]. However, a monoclinic distortion and domain structure that preserves chirality, which is needed to

explain the PGE results, can now explain the observed XNCD. Thus, simultaneous TRSB effects cannot be ruled out since the geometry of the experiment, with the x-ray wave vector in the c direction, may not be sensitive to magnetic effects with an in-plane order parameter, which in BSCCO appears concurrent with charge order at T^* [8,10].

On the other hand, a solely structural effect, even with the addition of the charge order transition, without TRSB is at odds with other experiments that specifically probe time-reversal and inversion-symmetry breaking. In particular, if we include magnetic moments (either spins or current loops), unless moments are intra-unit-cell, the $mm2$ structure breaks translational symmetry, which is inconsistent with neutron diffraction experiments. The polarized magnetic scattering [5,7,57] including Bi2212 [10] observes extra intensity below T^* at the $(1, 0, \ell)$ Bragg spots (and its equivalents due to domains) consistent with $m\underline{m}m$ (with twofold axis rotation around y [58]), and nothing at the much easier to observe $(1/2, 1/2, \ell)$ Bragg spots, which would be required for $mm2$ of any origin.

Second-harmonic generation (SHG) was also suggested [58] as an effective probe for bulk inversion symmetry breaking, and performed on $YBa_2Cu_3O_{6+x}$ (YBCO) [12]. The data over a wide doping range revealed a monoclinic crystal with symmetry $2/m$ (C_{2h}; only twofold proper rotation about the c axis and a mirror plane, rather than orthorhombic already above T^*, assumed to be due to disorder in the oxygen chains). The observed SHG was interpreted as an incoherent response from domains of point group symmetry $\underline{2}/m$, or $m\underline{1}$, smaller than the laser spot, that average out to maintain an observed C_2 symmetry below T^* [12]. Subsequent analysis of the same data [59] suggested a different interpretation, where signal from single domains with symmetry $m\underline{m}m$ is superimposed with a global mmm symmetry. This alternative possibility reflects the difficulty of determining the symmetry of these complex material systems. However, unlike BSCCO, in YBCO the charge order onsets below a characteristic temperature $T_{CO} < T^*$, and resembles more a crossover than a true order parameter, presumably partially due to disorder (see, e.g., phase diagram in [1]). At the same time, the expectation that the pseudogap is a universal phenomenon within the cuprates suggests that the transition that we observe in BSCCO at T^* will have similar origin to the sharp onset of order in SHG experiments on YBCO. This further implies that charge order alone cannot be the only explanation to the observed symmetry deduced from the PGE data below T^*. For example, $m\underline{1}$ observed in SHG in YBCO is a subgroup of $mm2\underline{1}$ observed in PGE in BSCCO, which could point to a similar origin of the pseudogap order parameter in the two materials.

Thus, the above discussion suggests that to understand the PGE results we need to consider mesoscopic domains of lower symmetry that when fused together continue to satisfy the required constraints from the data, particularly the chiral behavior. Assuming the same symmetry breaking as that observed in SHG, our data will be consistent with domains of $m\underline{1}$ rotated 90°, thus averaged out to yield the observed $mm2\underline{1}$ symmetry, while also allowing for an order parameter that is odd under time reversal. The lack of mirror symmetries along the c direction reflects the observed chirality, which could be unique to the BSCCO system, e.g., associated with distortions in the Bi-O layer [46]. As it is constrained to the Bi-O layers, it may not interfere with the intra-unit-cell loop order observed in neutron scattering.

Several different models exhibiting TRSB were proposed to explain the symmetry breaking below T^* [2,60–64]. However, to agree with our observed $mm2\underline{1}$ or $mm2$ symmetry, they must impose "domain fusing," which maintains coherence over the size of the sample to account for the magnitude of the effect we observe. As we discussed above, this may not be a simple task, since in general domain averaging tends to reduce a signal. A model that respects our observed symmetry and relies on topology to guarantee that PGE currents within domains add coherently was recently proposed in [65]. In that model, the four possible domains with internal current loop order with unit-cell $m\underline{m}m$ symmetry [60] observed in neutron scattering [10] are glued together subject to the requirement that currents at the domain boundaries are conserved leading to a unique supercell. The resulting boundary currents from domains of size of 5 or more lattice constants (see Fig. S8(c) in the SM [33]) respect our observed $mm2$ symmetry. Further discussion of this possibility is given in the SM [33].

Finally, with a magnetic origin for both, $mm2\underline{1}$ and $mm2$ equally well agree with the data. The former is the paramagnetic version of the latter, which would result if the moments were anisotropic and fluctuating on a timescale faster than the timescale of our measurements (or if instead of ordered moments there were ordered quadrupoles). This is reminiscent of the contrast between neutron scattering with a timescale of measurement smaller than 10^{-12} seconds over which order is observed [5,7,10,11] and μ-relaxation rate. The latter, which is also linear in the order parameter, observes an altered rate below T^*, from which an internal magnetic field below T^* fluctuating on a timescale of $O(10^{-7})$ seconds is deduced [66,67]. Our measurements are basically dc and would therefore be consistent with these results.

V. SUMMARY

In summary, through detailed observation of circular and linear photogalvanic effects we show that the transition to the pseudogap regime in two families of Bi-based cuprate superconductors marks a phase transition associated with the development of chiral and inversion symmetry breaking. Our results are shown to be consistent with previous neutron scattering results, while also explaining the previously puzzling observation of the onset of chirality below T^* [56]. While charge order, which for the BSCCO system was shown to occur at T^*, could potentially lower the crystal symmetry from orthorhombic to monoclinic, domain averaging will retain the robust chiral and inversion symmetry breaking, while exhibiting an effective domain symmetry consistent with the magnetic point groups $mm2\underline{1}$ and $mm2$. At the same time, searching for a common mechanism for the pseudogap in all cuprates, including YBCO, we must conclude that charge order transition in BSCCO may affect the observed symmetry, but is not the main cause of the pseudogap order parameter. We finally note that certain models of intra-unit-cell loop current order can reassemble into domains which is consistent with $mm2\underline{1}$ and $mm2$ symmetries, where the former

can explain the lack of observations of local magnetism at low frequencies, while the full intra-unit-cell antiferromagnetic loop order is observed at short (i.e., neutron scattering) timescales.

ACKNOWLEDGMENTS

The authors thank Yoshiyuki Yoshida for help with growing single crystals of Pb-Bi2201 previously characterized in [9], Nobuhisa Kaneko and Martin Greven for providing us single crystals of Bi2212 previously characterized in [28], and Benjamin Feldman for allowing us to use their argon-filled glove box equipped with a transfer station. Stimulating discussions with B. Spivak, D. Hsieh, S. Kivelson, T. Morimoto, and M. Norman are greatly appreciated. This work was supported by the U.S. Department of Energy, Office of Science, Basic Energy Sciences, Division of Materials Sciences and Engineering, under Contract No. DE-AC02-76SF00515. Device fabrication was partially supported by the Gordon and Betty Moore Foundation through Grant No. GBMF4529.

[1] B. Keimer, S. A. Kivelson, M. R. Norman, S. Uchida, and J. Zaanen, From quantum matter to high-temperature superconductivity in copper oxides, Nature (London) **518**, 179 (2015).

[2] C. M. Varma, Non-Fermi-liquid states and pairing instability of a general model of copper oxide metals, Phys. Rev. B **55**, 14554 (1997).

[3] S. Chakravarty, R. B. Laughlin, D. K. Morr, and C. Nayak, Hidden order in the cuprates, Phys. Rev. B **63**, 094503 (2001).

[4] E. Fradkin, S. A. Kivelson, and J. M. Tranquada, Colloquium: Theory of intertwined orders in high temperature superconductors, Rev. Mod. Phys. **87**, 457 (2015).

[5] B. Fauqué, Y. Sidis, V. Hinkov, S. Pailhès, C. T. Lin, X. Chaud, and P. Bourges, Magnetic Order in the Pseudogap Phase of High-T_c Superconductors, Phys. Rev. Lett. **96**, 197001 (2006).

[6] J. Xia, E. Schemm, G. Deutscher, S. A. Kivelson, D. A. Bonn, W. N. Hardy, R. Liang, W. Siemons, G. Koster, M. M. Fejer, and A. Kapitulnik, Polar Kerr-Effect Measurements of the High-Temperature $YBa_2Cu_3O_{6+x}$ Superconductor: Evidence for Broken Symmetry near the Pseudogap Temperature, Phys. Rev. Lett. **100**, 127002 (2008).

[7] H. A. Mook, Y. Sidis, B. Fauqué, V. Balédent, and P. Bourges, Observation of magnetic order in a superconducting $YBa_2Cu_3O_{6.6}$ single crystal using polarized neutron scattering, Phys. Rev. B **78**, 020506(R) (2008).

[8] A. Kaminski, S. Rosenkranz, H. M. Fretwell, J. C. Campuzano, Z. Li, H. Raffy, W. G. Cullen, H. You, C. G. Olson, C. M. Varma, and H. Höchst, Spontaneous breaking of time-reversal symmetry in the pseudogap state of a high-T_c superconductor, Nature (London) **416**, 610 (2002).

[9] R.-H. He, M. Hashimoto, H. Karapetyan, J. D. Koralek, J. P. Hinton, J. P. Testaud, V. Nathan, Y. Yoshida, H. Yao, K. Tanaka, W. Meevasana, R. G. Moore, D. H. Lu, S.-K. Mo, M. Ishikado, H. Eisaki, Z. Hussain, T. P. Devereaux, S. A. Kivelson, J. Orenstein *et al.*, From a single-band metal to a high-temperature superconductor via two thermal phase transitions, Science **331**, 1579 (2011).

[10] S. De Almeida-Didry, Y. Sidis, V. Balédent, F. Giovannelli, I. Monot-Laffez, and P. Bourges, Evidence for intra-unit-cell magnetic order in $Bi_2Sr_2CaCu_2O_{8+\delta}$, Phys. Rev. B **86**, 020504(R) (2012).

[11] L. Mangin-Thro, Y. Sidis, P. Bourges, S. De Almeida-Didry, F. Giovannelli, and I. Laffez-Monot, Characterization of the intra-unit-cell magnetic order in $Bi_2Sr_2CaCu_2O_{8+\delta}$, Phys. Rev. B **89**, 094523 (2014).

[12] L. Zhao, C. A. Belvin, R. Liang, D. A. Bonn, W. N. Hardy, N. P. Armitage, and D. Hsieh, A global inversion-symmetry-broken phase inside the pseudogap region of $YBa_2Cu_3O_y$, Nat. Phys. **13**, 250 (2017).

[13] R. Daou, J. Chang, D. LeBoeuf, O. Cyr-Choinière, F. Laliberté, N. Doiron-Leyraud, B. J. Ramshaw, R. Liang, D. A. Bonn, W. N. Hardy, and L. Taillefer, Broken rotational symmetry in the pseudogap phase of a high-T_c superconductor, Nature (London) **463**, 519 (2010).

[14] R. Comin, R. Sutarto, E. H. da Silva Neto, L. Chauviere, R. Liang, W. N. Hardy, D. A. Bonn, F. He, G. A. Sawatzky, and A. Damascelli, Broken translational and rotational symmetry via charge stripe order in underdoped $YBa_2Cu_3O_{6+y}$, Science **347**, 1335 (2015).

[15] Y. Sato, S. Kasahara, H. Murayama, Y. Kasahara, E.-G. Moon, T. Nishizaki, T. Loew, J. Porras, B. Keimer, T. Shibauchi, and Y. Matsuda, Thermodynamic evidence for a nematic phase transition at the onset of the pseudogap in $YBa_2Cu_3O_y$, Nat. Phys. **13**, 1074 (2017).

[16] C. Howald, H. Eisaki, N. Kaneko, M. Greven, and A. Kapitulnik, Periodic density-of-states modulations in superconducting $Bi_2Sr_2CaCu_2O_{8+\delta}$, Phys. Rev. B **67**, 014533 (2003).

[17] M. Vershinin, S. Misra, S. Ono, Y. Abe, Y. Ando, and A. Yazdani, Local ordering in the pseudogap state of the high-T_c superconductor $Bi_2Sr_2CaCu_2O_{8+\delta}$, Science **303**, 1995 (2004).

[18] W. D. Wise, M. C. Boyer, K. Chatterjee, T. Kondo, T. Takeuchi, H. Ikuta, Y. Wang, and E. W. Hudson, Charge-density-wave origin of cuprate checkerboard visualized by scanning tunnelling microscopy, Nat. Phys. **4**, 696 (2008).

[19] M. J. Lawler, K. Fujita, J. Lee, A. R. Schmidt, Y. Kohsaka, C. K. Kim, H. Eisaki, S. Uchida, J. C. Davis, J. P. Sethna, and E.-A. Kim, Intra-unit-cell electronic nematicity of the high-T_c copper-oxide pseudogap states, Nature (London) **466**, 347 (2010).

[20] C. V. Parker, P. Aynajian, E. H. da Silva Neto, A. Pushp, S. Ono, J. Wen, Z. Xu, G. Gu, and A. Yazdani, Fluctuating stripes at the onset of the pseudogap in the high-T_c superconductor $Bi_2Sr_2CaCu_2O_{8+x}$, Nature (London) **468**, 677 (2010).

[21] E. H. da Silva Neto, P. Aynajian, A. Frano, R. Comin, E. Schierle, E. Weschke, A. Gyenis, J. Wen, J. Schneeloch, Z. Xu, S. Ono, G. Gu, M. Le Tacon, and A. Yazdani, Ubiquitous interplay between charge ordering and high-temperature superconductivity in cuprates, Science **343**, 393 (2014).

[22] S. Mukhopadhyay, R. Sharma, C. K. Kim, S. D. Edkins, M. H. Hamidian, H. Eisaki, S. Uchida, E.-A. Kim, M. J. Lawler, A. P. Mackenzie, J. C. Davis, and K. Fujita, Evidence for a vestigial nematic state in the cuprate pseudogap phase, Proc. Natl. Acad. Sci. USA **116**, 13249 (2019).

[23] K. Ishida, S. Hosoi, Y. Teramoto, T. Usui, Y. Mizukami, K. Itaka, Y. Matsuda, T. Watanabe, and T. Shibauchi, Divergent nematic susceptibility near the pseudogap critical point in a cuprate superconductor, J. Phys. Soc. Jpn. **89**, 064707 (2020).

[24] Y. Y. Peng, M. Salluzzo, X. Sun, A. Ponti, D. Betto, A. M. Ferretti, F. Fumagalli, K. Kummer, M. Le Tacon, X. J. Zhou, N. B. Brookes, L. Braicovich, and G. Ghiringhelli, Direct observation of charge order in underdoped and optimally doped $Bi_2(Sr,La)_2CuO_{6+\delta}$ by resonant inelastic x-ray scattering, Phys. Rev. B **94**, 184511 (2016).

[25] V. I. Belinicher and B. I. Sturman, The photogalvanic effect in media lacking a center of symmetry, Sov. Phys. Usp. **23**, 199 (1980).

[26] B. I. Sturman and V. M. Fridkin, *The Photovoltaic and Photorefractive Effects in Noncentrosymmetric Materials* (Gordon and Breach, Philadelphia, 1992).

[27] S. D. Ganichev and W. Prettl, Spin photocurrents in quantum wells, J. Phys.: Condens. Matter **15**, R935 (2003).

[28] A. Fang, C. Howald, N. Kaneko, M. Greven, and A. Kapitulnik, Periodic coherence-peak height modulations in superconducting $Bi_2Sr_2CaCu_2O_{8+\delta}$, Phys. Rev. B **70**, 214514 (2004).

[29] Using notations of Birss [44] in considering the effect of time inversion, we identify CPGE with an "i" tensor and LPGE with a "c" tensor.

[30] J. Hwang, T. Timusk, and G. D. Gu, Doping dependent optical properties of $Bi_2Sr_2CaCu_2O_{8+\delta}$, J. Phys.: Condens. Matter **19**, 125208 (2007).

[31] E. van Heumen, W. Meevasana, A. B. Kuzmenko, H. Eisaki, and D. van der Marel, Doping-dependent optical properties of Bi2201, New J. Phys. **11**, 055067 (2009).

[32] W. Ruan, C. Hu, J. Zhao, P. Cai, Y. Peng, C. Ye, R. Yu, X. Li, Z. Hao, C. Jin, X. Zhou, Z.-Y. Weng, and Y. Wang, Relationship between the parent charge transfer gap and maximum transition temperature in cuprates, Sci. Bull. **61**, 1826 (2016).

[33] See Supplemental Material at http://link.aps.org/supplemental/10.1103/PhysRevB.105.155103 for details on the device characterization and data analysis.

[34] E. Sterpetti, J. Biscaras, A. Erb, and A. Shukla, Comprehensive phase diagram of two-dimensional space charge doped $Bi_2Sr_2CaCu_2O_{8+x}$, Nat. Commun. **8**, 2060 (2017).

[35] Y. He, M. Hashimoto, D. Song, S.-D. Chen, J. He, I. M. Vishik, B. Moritz, D.-H. Lee, N. Nagaosa, J. Zaanen, T. P. Devereaux, Y. Yoshida, H. Eisaki, D. H. Lu, and Z.-X. Shen, Rapid change of superconductivity and electron-phonon coupling through critical doping in Bi-2212, Science **362**, 62 (2018).

[36] M. D. Kirk, C. B. Eom, B. Oh, S. R. Spielman, M. R. Beasley, A. Kapitulnik, T. H. Geballe, and C. F. Quate, Scanning tunneling microscopy of the *a-b* planes of $Bi_2(Ca,Sr)_3Cu_2O_{8+\delta}$ single crystal and thin film, Appl. Phys. Lett. **52**, 2071 (1988).

[37] J. W. McIver, D. Hsieh, H. Steinberg, P. Jarillo-Herrero, and N. Gedik, Control over topological insulator photocurrents with light polarization, Nat. Nanotechnol. **7**, 96 (2012).

[38] P. A. Miles, S. J. Kennedy, G. J. McIntyre, G. D. Gu, G. J. Russell, and N. Koshizuka, Refinement of the incommensurate structure of high quality Bi-2212 single crystals from a neutron diffraction study, Phys. C (Amsterdam) **294**, 275 (1998).

[39] A. Mans, I. Santoso, Y. Huang, W. K. Siu, S. Tavaddod, V. Arpiainen, M. Lindroos, H. Berger, V. N. Strocov, M. Shi, L. Patthey, and M. S. Golden, Experimental Proof of a Structural Origin for the Shadow Fermi Surface of $Bi_2Sr_2CaCu_2O_{8+\delta}$, Phys. Rev. Lett. **96**, 107007 (2006).

[40] S. Di Matteo and M. R. Norman, X-ray dichroism and the pseudogap phase of cuprates, Phys. Rev. B **76**, 014510 (2007).

[41] E. Deyo, L. E. Golub, E. L. Ivchenko, and B. Spivak, Semiclassical theory of the photogalvanic effect in non-centrosymmetric systems, arXiv:0904.1917.

[42] L. E. Golub, E. L. Ivchenko, and B. Spivak, Semiclassical theory of the circular photogalvanic effect in gyrotropic systems, Phys. Rev. B **102**, 085202 (2020).

[43] S.-Y. Xu, Q. Ma, Y. Gao, A. Kogar, A. Zong, A. M. Mier Valdivia, T. H. Dinh, S.-M. Huang, B. Singh, C.-H. Hsu, T.-R. Chang, J. P. C. Ruff, K. Watanabe, T. Taniguchi, H. Lin, G. Karapetrov, D. Xiao, P. Jarillo-Herrero, and N. Gedik, Spontaneous gyrotropic electronic order in a transition-metal dichalcogenide, Nature (London) **578**, 545 (2020).

[44] R. R. Birss, *Symmetry and Magnetism* (North-Holland, Amsterdam, 1964).

[45] I. Zeljkovic, E. J. Main, T. L. Williams, M. C. Boyer, K. Chatterjee, W. D. Wise, Y. Yin, M. Zech, A. Pivonka, T. Kondo, T. Takeuchi, H. Ikuta, J. Wen, Z. Xu, G. D. Gu, E. W. Hudson, and J. E. Hoffman, Scanning tunnelling microscopy imaging of symmetry-breaking structural distortion in the bismuth-based cuprate superconductors, Nat. Mater. **11**, 585 (2012).

[46] R. E. Gladyshevskii and R. Flükiger, Modulated structure of $Bi_2Sr_2CaCu_2O_{8+\delta}$, a high-$T_c$ superconductor with monoclinic symmetry, Acta Crystallogr., Sect. B: Struct. Sci. **52**, 38 (1996).

[47] R. Lifshitz, Magnetic point groups and space groups, in *Encyclopedia of Condensed Matter Physics*, edited by F. Bassani, G. L. Liedl, and P. Wyder (Elsevier Science, Oxford, 2005), pp. 219–226.

[48] X. B. Kan and S. C. Moss, Four-dimensional crystallographic analysis of the incommensurate modulation in a $Bi_2Sr_2CaCu_2O_8$ single crystal, Acta Crystallogr., Sect. B: Struct. Sci. **48**, 122 (1992).

[49] S. A. Kivelson, E. Fradkin, and V. J. Emery, Electronic liquid-crystal phases of a doped Mott insulator, Nature (London) **393**, 550 (1998).

[50] S. A. Kivelson, I. P. Bindloss, E. Fradkin, V. Oganesyan, J. M. Tranquada, A. Kapitulnik, and C. Howald, How to detect fluctuating stripes in the high-temperature superconductors, Rev. Mod. Phys. **75**, 1201 (2003).

[51] M. Vojta, Lattice symmetry breaking in cuprate superconductors: Stripes, nematics, and superconductivity, Adv. Phys. **58**, 699 (2009).

[52] E. Fradkin, S. A. Kivelson, M. J. Lawler, J. P. Eisenstein, and A. P. Mackenzie, Nematic Fermi fluids in condensed matter physics, Annu. Rev. Condens. Matter Phys. **1**, 153 (2010).

[53] V. M. Asnin, A. A. Bakun, A. M. Danishevskii, E. L. Ivchenko, G. E. Pikus, and A. A. Rogachev, "Circular" photogalvanic effect in optically active crystals, Solid State Commun. **30**, 565 (1979).

[54] S. S. Tsirkin, P. A. Puente, and I. Souza, Gyrotropic effects in trigonal tellurium studied from first principles, Phys. Rev. B **97**, 035158 (2018).

[55] A. V. Andrianov, E. L. Ivchenko, G. E. Pikus, R. Ya. Rasulov, and I. D. Yaroshetski, Linear photogalvanic effect in *p*-type A_3B_5 crystals, Ferroelectrics **43**, 177 (1982).

[56] M. Kubota, K. Ono, Y. Oohara, and H. Eisaki, X-ray optical activity in underdoped Bi-based high-T_c superconductor, J. Phys. Soc. Jpn. **75**, 053706 (2006).

[57] Y. Li, V. Balédent, N. Barišić, Y. Cho, B. Fauqué, Y. Sidis, G. Yu, X. Zhao, P. Bourges, and M. Greven, Unusual magnetic order in the pseudogap region of the superconductor $HgBa_2CuO_{4+\delta}$, Nature (London) **455**, 372 (2008).

[58] M. E. Simon and C. M. Varma, Symmetry considerations for the detection of second-harmonic generation in cuprates in the pseudogap phase, Phys. Rev. B **67**, 054511 (2003).

[59] A. de la Torre, K. L. Seyler, L. Zhao, S. Di Matteo, M. S. Scheurer, Y. Li, B. Yu, M. Greven, S. Sachdev, M. R. Norman, and D. Hsieh, Mirror symmetry breaking in a model insulating cuprate, Nat. Phys. **17**, 777 (2021).

[60] M. E. Simon and C. M. Varma, Detection and Implications of a Time-Reversal Breaking State in Underdoped Cuprates, Phys. Rev. Lett. **89**, 247003 (2002).

[61] C. M. Varma, Theory of the pseudogap state of the cuprates, Phys. Rev. B **73**, 155113 (2006).

[62] V. M. Yakovenko, Tilted loop currents in cuprate superconductors, Phys. B (Amsterdam) **460**, 159 (2015).

[63] S. W. Lovesey, D. D. Khalyavin, and U. Staub, Ferro-type order of magneto-electric quadrupoles as an order-parameter for the pseudo-gap phase of a cuprate superconductor, J. Phys.: Condens. Matter **27**, 292201 (2015).

[64] M. Fechner, M. J. A. Fierz, F. Thöle, U. Staub, and N. A. Spaldin, Quasistatic magnetoelectric multipoles as order parameter for pseudogap phase in cuprate superconductors, Phys. Rev. B **93**, 174419 (2016).

[65] C. M. Varma, Pseudogap and Fermi arcs in underdoped cuprates, Phys. Rev. B **99**, 224516 (2019).

[66] J. Zhang, Z. Ding, C. Tan, K. Huang, O. O. Bernal, P.-C. Ho, G. D. Morris, A. D. Hillier, P. K. Biswas, S. P. Cottrell, H. Xiang, X. Yao, D. E. MacLaughlin, and L. Shu, Discovery of slow magnetic fluctuations and critical slowing down in the pseudogap phase of $YBa_2Cu_3O_y$, Sci. Adv. **4**, eaao5235 (2018).

[67] S. Gheidi, K. Akintola, A. C. Y. Fang, S. Sundar, A. M. Côté, S. R. Dunsiger, G. D. Gu, and J. E. Sonier, Absence of μSR evidence for magnetic order in the pseudogap phase of $Bi_{2+x}Sr_{2-x}CaCu_2O_{8+\delta}$, Phys. Rev. B **101**, 184511 (2020).